applied sciences

MDPI

Article

Analysis and Optimization of the Performances of the Tandem Blade Radial Compressor Using the CFD

Mustafa Erturk Soylemez [1,*], Rasim Behçet [2] and Zekeriya Parlak [3]

[1] Department of Mechanical Engineering, Faculty of Engineering and Architectural, Muş Alparslan University, 49250 Muş, Türkiye
[2] Department of Mechanical Engineering, Faculty of Engineering, Inönü University, 44280 Malatya, Türkiye; rasim.behcet@inonu.edu.tr
[3] Department of Mechanical Engineering, Faculty of Engineering, Sakarya University, 54050 Serdivan, Türkiye; zparlak@sakarya.edu.tr
* Correspondence: e.soylemez@alparslan.edu.tr

Abstract: Centrifugal compressors are frequently used in both military and commercial areas because they can be easily manufactured and reach high-pressure compression ratios. The factor that limits the performance and operating range of compressors is flow instability. Many ideas have been put forward for performance improvement, but tandem blade radial compressors, which do not require an extra air system, have attracted the most interest. In this study, computational fluid dynamics (CFD) analyses were carried out on various parameters of the tandem blade (TB) radial compressor, and an optimization study was carried out to find the best design using a genetic algorithm on a whole operating curve. It was investigated how these parameters affected the efficiency and total pressure ratio between the determined lower and upper limits. The numerical analyses of the optimum design obtained as a result of the iterations were carried out. As a result of the iterations, three optimum designs were obtained and numerical analysis was carried out according to one of them, and then they were compared with the results in the literature. The general agreement of computational fluid dynamics and the literature data served as a validation for the computational approach. The error rates between the numerical analysis results and the experimental results in the literature were calculated for different flow rates and were found to be 1.98% as the highest and 0.35 as the lowest. The work carried out in this article will provide a valuable reference for future advanced tandem blade compressor designs.

Keywords: radial compressor; tandem blade; modelling; optimization; CFD

Citation: Soylemez, M.E.; Behçet, R.; Parlak, Z. Analysis and Optimization of the Performances of the Tandem Blade Radial Compressor Using the CFD. *Appl. Sci.* **2024**, *14*, 4256. https://doi.org/10.3390/app14104256

Academic Editor: Jianzhong Lin

Received: 18 April 2024
Revised: 11 May 2024
Accepted: 14 May 2024
Published: 17 May 2024

1. Introduction

Compressors are essential in the processes required for pressurizing and transporting gases and liquids in industry, aerospace applications, and civil and military fields. It is one of the basic equipment of the heating, ventilation, and air conditioning systems for houses and other structures [1]. Compressors can be classified into two basic types: positive displacement and dynamic. Positive displacement compressors are divided into four: piston, screw, vane, and lobe compressors. Dynamic compressors are divided into two: axial and radial compressors [2]. Radial compressors increase the kinetic energy of the fluid with the help of a rotating impeller [3]. Many design optimizations and numerical analyses have been used to improve compressor aerodynamic designs and increase their performance [4–10]. Hadavandi et al. aimed to improve compressor CFD by providing a complete set of input data for numerical simulations [11]. Shaban aimed to improve radial compressor performance by optimizing the design of the radial bladeless diffuser. It was proposed, investigated, and numerically optimized to be two bladeless diffuser geometries. The main goal of the optimization was to increase the pressure coefficient and minimize the diffuser loss coefficient. The diffuser reduced the loss coefficient by up to

10 percent and increased the pressure coefficient by 3.8 percent. He performed the simulations by solving the Reynolds-averaged Navier–Stokes equation under 2D axisymmetric conditions [12]. Based on the ANSYS CFX Version 18.0 workbench finite element analysis software, Sun et al. investigated the numerical simulation of the fluid–solid coupling of pipeline radial compressor impeller by the unstructured grid finite volume method and finite element method. They numerically analyzed the equivalent stress distribution caused by the radial load of the impeller, and the coupling effect of radial load and aerodynamic load [13]. Xu et al. used a low-flow, single-stage centrifugal compressor with a bladeless diffuser to investigate the position effects of the splitter blade between the two main blades. Splitter blade position optimizations were carried out numerically. They stated that the splitter blade positions are influential on the compressor stage performances. They stated that the traditional splitter blade located in the middle of the two main blades is not the most suitable position for aerodynamic performance [14]. Li et al. examined the mathematical model of the flow field of the radial compressor, which is one of the basic components of the turbocharger. They stated that when the number of grids in a single channel is over 300,000, the increase in the number of grids has little effect on the compressor performance. They stated that the numerical simulation method they used could be used to predict compressor performance, and the total pressure ratio difference between calculation and test was less than 7% [15]. Aghaei et al. aimed to show how a good compressor can be designed and modeled with CFD stable models and to explain the reasons for the discrepancies between experiment (1D design) and 3D CFD analysis. They found a good match between CFD and one-dimensional data for a radial impeller with a pressure ratio of approximately 4:1. They stated that, in general, CFD gives a good estimate of performance and adequately resolves local flow details [16]. Roberts et al. performed a parametric study of the clocking between the TB inducer/exducer to investigate its impact on performance and output stream quality. They showed that the relative environmental position or clock setting between the inducer/exducer has a remarkable effect on TB performance. They noted that the maximum change in operating blade efficiency estimated for various TB configurations was approximately 3.8 [17]. Cuturi et al. designed and simulated a TB radial compressor for hybrid compound turbocharging. They developed the configurations through a series of improvements guided by the design of experiments (DOE). Full 3D CFD simulations were performed at three different speeds: 2000 rpm, 3500 rpm, and 5500 rpm, respectively. They noted that the final geometry had a higher pressure ratio than the original unit, an improved surge margin, and a lower sensitivity to choke [18]. Noman et al. present a comprehensive experimental and numerical study on the performance of a medium pressure ratio, shrouded, TB centrifugal compressor compared to a conventional compressor used commercially in China for turbocharging applications. They stated that in all tandem design cases, the surge point shifts towards lower mass flow rates. They stated that a maximum increase of 25 percent was observed in the study range. They emphasized that when a 20 percent reduction in inducer thickness was made, it performed better than conventional designs [19]. Ju et al. used the CFD method to examine the specific aerodynamic performance of the TB. They said that compared to a single-row blade, a tandem row has the potential to produce a higher pressure ratio with lower losses over a relatively narrow operating range [20]. Josuhn-Kadner studied the effect of TB geometry on rotor and stage characteristics. He performed measurements at nine points all around the rotor, taking into account three different environmental inducer positions. He stated that the improvement achieved by the TB configuration in the rotor and stage characteristics was slight. Still, there were major differences in the flow field at the rear and outlet of the rotor [21]. Josuhn-Kadner et al. have mainly investigated experimentally for radial compressor aerodynamic stage optimization. They developed 3D Navier–Stokes calculations in the design to analyze the flow field. They said the inducer setting has a negligible effect on the rotor characteristics. They stated that the maximum rotor efficiency of 93.5% varies within less than 1% depending on different positions of the inducer [22]. Li et al. improved the compressor performance in highly loaded transonic radial compressors with a TB

impeller configuration with rule-surface inducer and exducer blades. Both the impeller and the diffuser achieved a compressor efficiency of 1.4% by reducing flow loss. They stated that using a forward sweep and negative lean design for the impeller, depending on the tandem impeller configuration, would increase efficiency by 2.11 percent compared to a conventional compressor. They said that diffuser performance can be improved with a negative lean design [23]. Li et al. first examined the flow characteristics of the conventional impeller to determine the causes of compressor instability. Then, they examined the TB impeller and showed the performance of different impellers. They particularly emphasized the variation in impeller tip leakage flow and impeller leading edge separation flow as the mechanism underlying the compressor operating range [24]. Sadagopan et al. described the mean-line procedure based on isentropic equations for the mixed flow case. They conducted rotor design evaluation studies for 3.5 kg/s mass flow by performing mean-line code and computational analysis based on Bezier curves. They stated that a higher hub load would result in a higher performance of the impeller with a lower tip leakage loss and regular flow at the outlet [25]. Sadagopan et al. computationally evaluated a supersonic mixed-flow compressor stage with a high-pressure ratio of 6:1 and an efficiency of 75.5%. They carried out the analysis by taking into account the effects of three-dimensionality, viscous flow, and compressibility. They described a new tandem design supersonic diffuser. They stated that this new design outperformed previous supersonic diffusion configurations by 20% in terms of efficiency [26]. Cravero et al. simulated a two-stage back-to-back radial compressor for refrigerant applications using computational fluid dynamics techniques at operating points close to the surge point. They confirmed the numerical results with experimental results [27]. Zhu et al. carried out CFD analysis on the optimization of low- and high-pressure radial compressors in a land-use MW-level gas turbine. They increased the pressure ratio and efficiency by reducing the blade diffuser diameter ratio for the low-pressure radial compressor. They stated that they reduced the deviation angle by using a diffuser with splitter blades for the high-pressure radial compressor and thus increased its performance [28]. Various numerical analysis studies have been carried out to improve the stall margin of the axial compressor [29–31].

In this study, optimization studies for some parameters of the TB radial compressor were carried out numerically. It has been observed that there is a lack of studies on the optimization of these parameters in the literature. The main goal of this paper is to investigate the effect of input parameters determined on pressure–compression ratio and efficiency in tandem blade radial compressors. To ensure the accuracy of the numerical analyses in the optimization studies, the results of the conventional blade centrifugal compressor, whose test results were available in the literature, were examined and confirmed with numerical analyses. After ensuring that our analyses worked, the numerical calculations of the TB centrifugal compressor were performed. The main goal of the optimization studies was to increase the efficiency and total pressure ratio. This goal was achieved with three optimum designs obtained from the analysis results.

2. Methodology

To examine the effects of the design parameters of the TB centrifugal compressor on performance, we first wanted to make sure that our analysis was correct. For this purpose, an industrial-sized compressor, whose test rig was designed and built by the University of Virginia Rotating Machinery and Control Laboratory (ROMAC), was chosen to verify the numerical studies in this study. They set up the experimental set as shown in Figure 1 [1].

Figure 1. Test set up [1].

The experimental system established includes a radial compressor, piping system, diffuser, and flow control devices. The design parameters of the selected radial compressor are shown in Table 1 [1]. They operated the compressor, which they designed for a speed of 23,000 rpm, at 17,000 rpm. They stated that the reason for this is that the high-speed electric motor connected to the compressor shaft can rotate the rotor at a maximum of 17,473 rpm. That is why we used 17,473 rpm in our analysis. In Figure 2, the design geometries are shown on the radial impeller sketch.

Table 1. Compressor design parameters [1].

Parameter	Value
Maximum speed (RPM)	23,000
Design mass flow rate (kg/s)	0.833
Design pressure ratio	1.68
Inducer hub diameter (mm)	56.3
Inducer tip diameter (mm)	116.72
Impeller tip diameter (mm)	250
Piping diameter (m)	0.203
Inlet piping length (m)	5.2
Exhaust piping length (m)	21.3

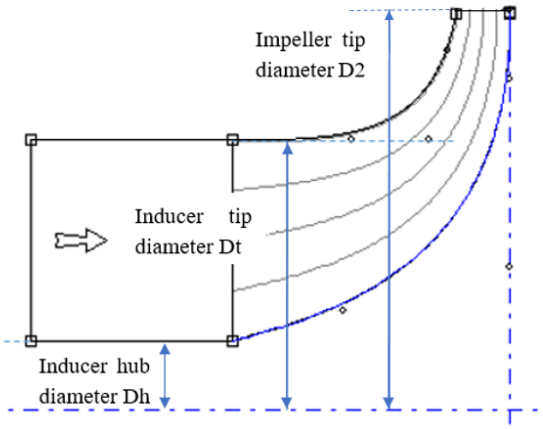

Figure 2. Impeller design geometry sketch.

They carried out the necessary data measurements using 12 pressure transducers in the test setup and also used a flow meter for flow control. They obtained measurements by placing these pressure transducers and thermocouples in the inlet, inside the compressor casing and outlet pipes.

A methodology has been created by examining the research conducted to facilitate the radial compressor design process. Using this methodology, the compressor can be designed parametrically according to the desired characteristics. The design methodology is given in Figure 3.

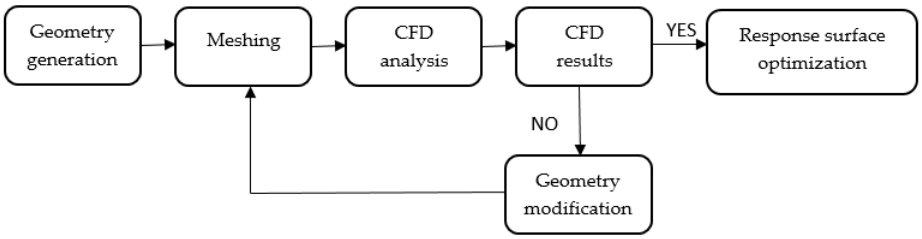

Figure 3. The outline of the design methodology.

2.1. Numerical Method and Validation

Vista Centrifugal Compressor Design (Vista CCD), available in ANSYS Workbench, was used to design the radial compressor. The design inputs of the compressor, shaft speed, mass flow rate, pressure ratio, air inlet temperature, and pressure were entered. In the continuation of the same module, geometric measurements, hub diameter, shroud diameter, the number of blades, and tip clearance values were entered. A compressor with 0.254 mm tip clearance and 18 blades without intermediate blades was designed as the number of blades. A mesh structure suitable for the design was created using the Turbogrid module. The normal distance option was selected by checking the override upstream geometry options. Automatic was selected for topology settings. The global size factor method was used for the mesh structure, and the method proportional to the mesh size was used for boundary layer improvement control. The absolute method was used for the element size near the wall. Figure 4 shows the mesh structure.

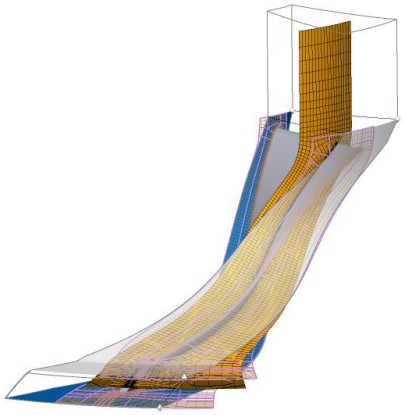

Figure 4. Mesh structure.

In Turbogrid, mesh statistics are used to see the quality of the mesh. Thus, the quality parameters of the created mesh such as minimum surface angle, maximum surface angle, maximum element volume ratio, and minimum volume ratio were examined. Percentage distortions were checked for entry, exit, and passage, and all were achieved with zero percent error. The minimum surface angle was 22.23° and the maximum surface angle was 160.72°.

Conservation equations for each element created were solved by the program. For a compressible, steady-state, homogeneous, and Newtonian fluid, the continuity, momentum, and energy equations can, respectively, be written as follows [32]:

Continuity equation:

$$\frac{\partial \rho}{\partial t} + \frac{\partial}{\partial xj}\left(\rho U_j\right) = 0 \quad (1)$$

Momentum equation:

$$\frac{\partial(\rho Ui)}{\partial t} + \frac{\partial}{\partial xj}\left(\rho U_i U_j\right) = -\frac{\partial p'}{\partial xj} + \frac{\partial}{\partial xj}\left[(\mu + \mu_t)\left(\frac{\partial Ui}{\partial xj} + \frac{\partial Uj}{\partial xj}\right)\right] + S_M \quad (2)$$

where S_M is the sum of body forces, μ_t is turbulent viscosity, and p' is the modified pressure.

Energy equation:

$$\frac{\partial(\rho h_e)}{\partial t} - \frac{\partial p}{\partial t} + \frac{\partial}{\partial t}\left(\rho U_j h_e\right) = \frac{\partial}{\partial xj}\left(\lambda \frac{\partial T}{\partial xj} - \rho\, \overline{u_j h_e}\right) + \frac{\partial}{\partial xj}\left[U_i\left(\tau_{ij} - \rho\, \overline{u_i u_j}\right)\right] \quad (3)$$

Which is suitable for flows and can be useful for liquids and gases in ANSYS CFX. The term $\rho\, \overline{u_j h_e}$ is additional turbulence flux and the $\frac{\partial}{\partial xj}\left[U_i\left(\tau_{ij} - \rho\, \overline{u_i u_j}\right)\right]$ term in the equation is the viscous work term. Symbol h_e is the enthalpy, and λ is thermal conductivity.

After the mesh structure was created, computational fluid dynamics analyses were performed using CFX-Pre. In order to analyze the experimental studies in the literature, the same inlet and outlet sections were designed and analyses were carried out as a vaneless diffuser, as in the literature. In the ANSYS CFX module, the radial compressor and coordinate system are defined as the machine type. Steady-state and compressible flow properties were preferred as analysis types. Rotation and speed as 17,473 rpm were entered as the component type. As for the wall structure, the tip clearance at the shroud was marked yes, and the tip clearance at the hub was marked no. Ideal air was chosen as physical definitions, reference pressure was chosen as 0 atm, heat transfer was chosen as total energy, and turbulence was chosen as shear–stress transport (SST). The SST turbulence model with automatic wall function treatment was used because of its highly accurate predictions of flow separation. In this model, the Reynolds stress terms in the momentum equations are treated using the shear–stress transport turbulence model, in which the k-w model is used in the near-wall region and the k-e model is implemented for the far field region [33]. The inlet pressure and temperature were entered as 101,325 Pa and 288.15 K, respectively. The total mass flow rate of the compressor was entered as 0.789 kg/s. As boundary conditions, a non-slip wall was chosen for the blade and hub, and a counter-rotating wall was chosen for the shroud. The advection scheme was chosen as the high-resolution, first-order turbulence number option in the solver controls. The convergence criterion was set to RMS 10^{-5}. Table 2 gives detailed boundary conditions and methodology. After the necessary settings are made, the CFX visual for a single blade of our radial compressor is shown in Figure 5.

Table 2. Details of the CFD numerical methodology and boundary conditions.

Solver	ANSYS CFX
Turbulence model	Shear–stress transport
Convergence criterion	Total residue < 10^{-5}
Inlet total pressure	101,325 Pa
Inlet total temperature	288.15 K
Solid wall	Nonslip and adiabatic boundary conditions
Periodic surface	Periodic boundary condition

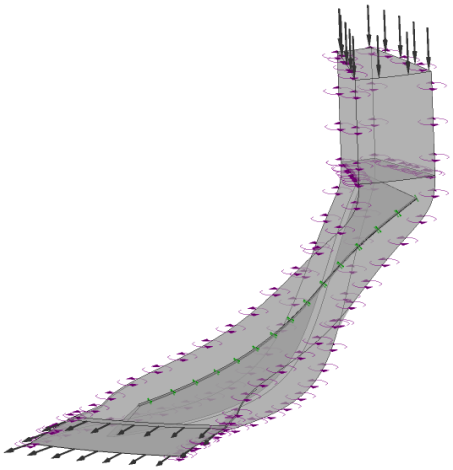

Figure 5. CFX setup.

Various analyses were performed to obtain mesh independence. These analyses were examined according to the change in total pressure ratio and the results are shown in Figure 6. In the graph below, it is seen that after the number of cells reaches 289,045, the output values of the problem reach a constant value and become independent of the number of mesh. Considering this graph, the network structure containing 289,045 cells is considered sufficient.

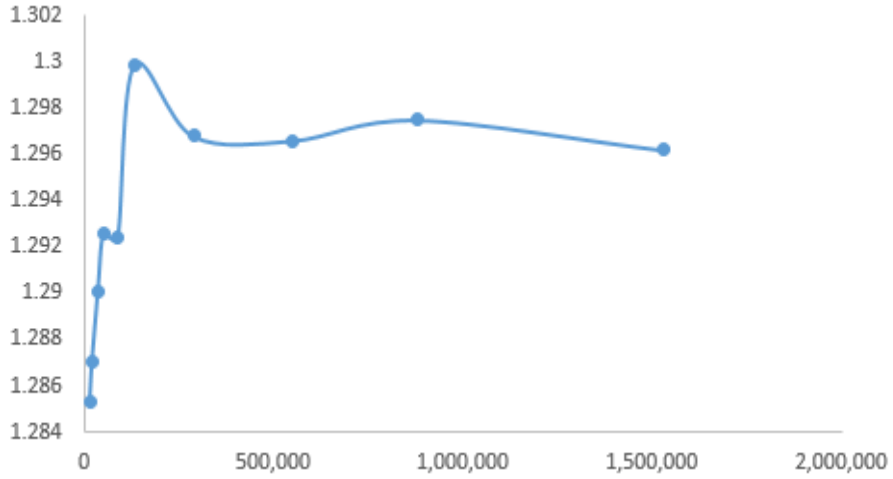

Figure 6. Graphical representation of mesh independence.

Many active and passive flow control ideas such as adjustable inlet guides, air jet injection, and vortex generation have been tried to increase the operating range, total pressure ratio, and efficiency of radial compressors. However, due to some deficiencies in these methods, they are far from applicability. Therefore, the tandem blade design, which is a more innovative idea, has attracted the attention of researchers.

2.2. Tandem Blade Radial Compressor

The TB radial compressor consists of blades arranged in two rows. The design of the TB radial compressor was made in the design modeler module of the ANSYS. The inducer and exducer parts of the TB impeller were created using the revolve feature in the design modeler module. The designed blade was transferred to the meshing module using the export point feature. Figure 7 shows the design of the tandem blade geometry.

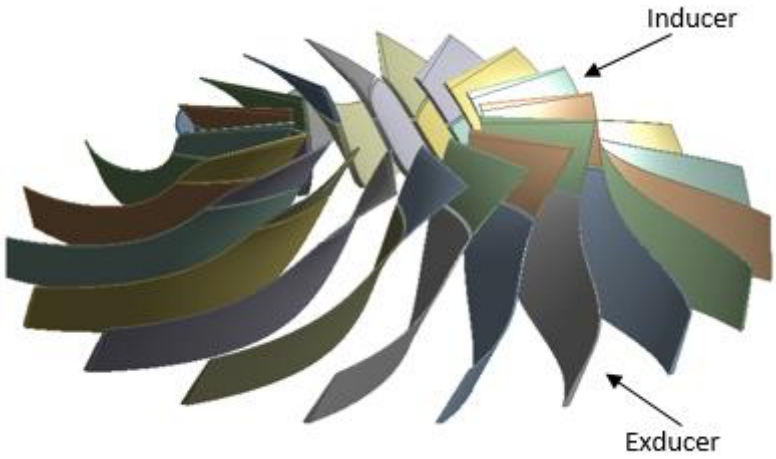

Figure 7. Tandem blade radial compressor design.

The design was transferred to the Turbogrid module to create the appropriate mesh and the mesh structure was created. The mesh structure was created for both the blades and the fluid. Figure 8 shows the mesh structure of the tandem compressor.

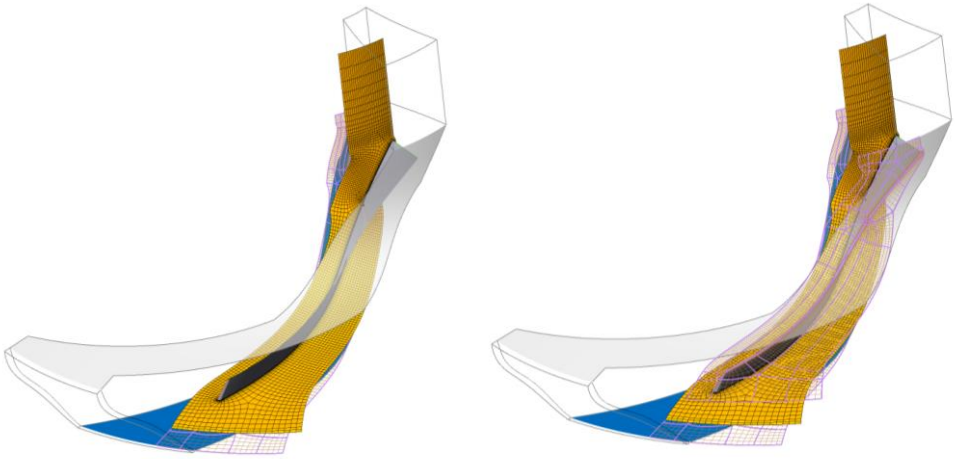

Figure 8. Mesh structure created for a tandem blade radial compressor.

The mesh structure of a single-blade flow path is shown to save time and energy. Two visuals were used to understand the shroud mesh structure. The analysis results were carried out for all blades of the impeller.

2.3. Parameter Optimization

Parameters that were thought to have an impact on performance were selected from the literature studies, and their effects on the performance of the TB centrifugal compressor were examined. Optimization operations were carried out on the desired parameters. Four input parameters were chosen. The cutoff angle between the inducer and exducer, theta; the vertical distance between the lower edge of the inducer and the upper edge of the exducer, which we call x; the rotational angle between the lower edge of the inducer and the upper edge of the exducer, clocking; and the vertical height of the inducer, length. As performance parameters, pressure ratio (Pr) and efficiency (μ) were chosen, which we checked from the results. The representation of the parameters on the tandem blade is shown in Figures 9 and 10.

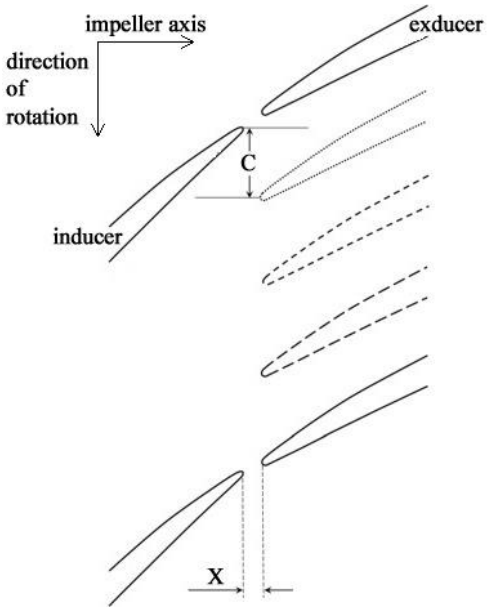

Figure 9. Representation of the X and C parameters.

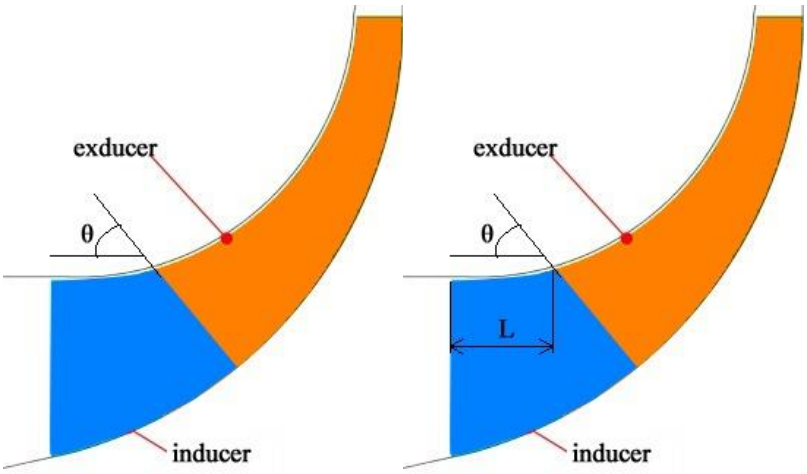

Figure 10. Representation of the θ and L parameters.

These four parameters were transferred to the response surface optimization tool, an ANSYS optimization module. The goal of this optimization is to enhance the total pressure ratio and efficiency. Given the dual optimization objectives, the design falls under the domain of multi-objective optimization problems. Multi-objective optimization does not aim to identify the absolute optimal solution; instead, it seeks a range of relatively optimal solutions. Genetic algorithms, renowned for their robust global optimization capabilities, stand out as effective tools for resolving multi-objective optimization problems arising from conflicting objectives. As a result, genetic algorithms were employed in this design for optimization purposes. NSGA-II (Non-dominated ranked genetic algorithm II) stands out as a highly utilized genetic algorithm. This approach introduces the crowding ranking criterion, organizing individuals within the population based on their dominant relationships prior to the execution of the selection operator. The flow chart of the NSGA-II algorithm is shown in Figure 11.

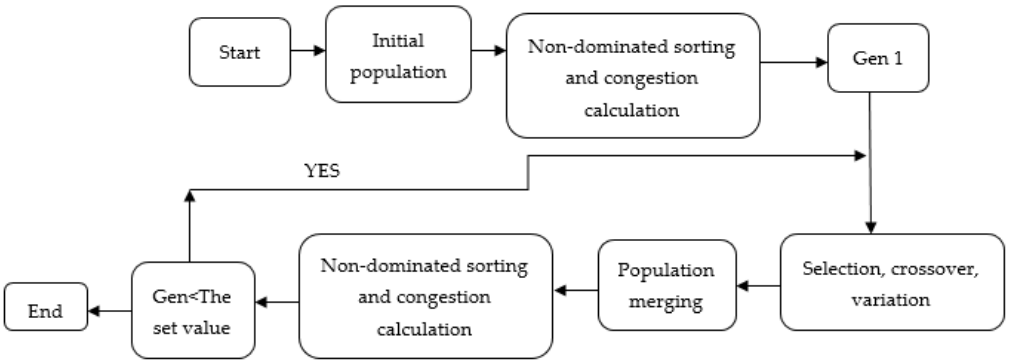

Figure 11. NSGA-II algorithm flow chart.

The output parameters we want to see the results of are also defined in this module. The output parameters vital to us are the total pressure ratio and efficiency. The lower and upper limits for the specified input parameters were determined by looking at the studies and taking into account the tandem blade geometry. Table 3 shows the lower and upper limits determined for our input parameters X, C, L, and θ.

Table 3. Lower and upper limits of input parameters.

Input Parameters	Lower Limits	Upper Limits
X (mm)	1.0	3.0
C (°)	0	10
L (mm)	15.0	25.0
θ (°)	60	105

3. Results and Discussion

We obtained the analysis results of the radial compressor, whose experimental results are in the literature. The analysis results of the compressor are shown below. Table 4 shows the performance results of the radial compressor for which we performed numerical analysis.

Table 4. Compressor performance results.

Parameter	Value
Rotation speed (rad/s)	1829.77
Inlet volume flow rate (m^3/s)	0.6578
Mass flow rate (kg/s)	0.8056
Work input coefficient	0.5721
Input power (W)	19,438.8
Total temperature ratio	1.0834
Total pressure ratio	1.2999
Total isentropic efficient	93.3362

Figures 12 and 13 are given for the plane projection of the meridional section. Figure 12 shows 50% velocity vectors. It can be seen that the flow follows the airfoil, creating a regular flow field. It is seen that the speed decreases locally due to the vortices formed at the blade exits due to the tip gap. It does not appear to exhibit any unexpected behavior.

The total pressure contour is given in Figure 13. It is seen that the total pressure is the lowest at the blade inlets, and the total pressure is at the highest level at the blade exit. It is seen that the total pressure is at the highest level where the speed at the blade exits is low. The consistency of the results obtained is important for the accuracy of the design.

The results of our radial compressor, which we designed and numerically analyzed, and the radial compressor, whose experimental results are in the literature, are shown in Table 5.

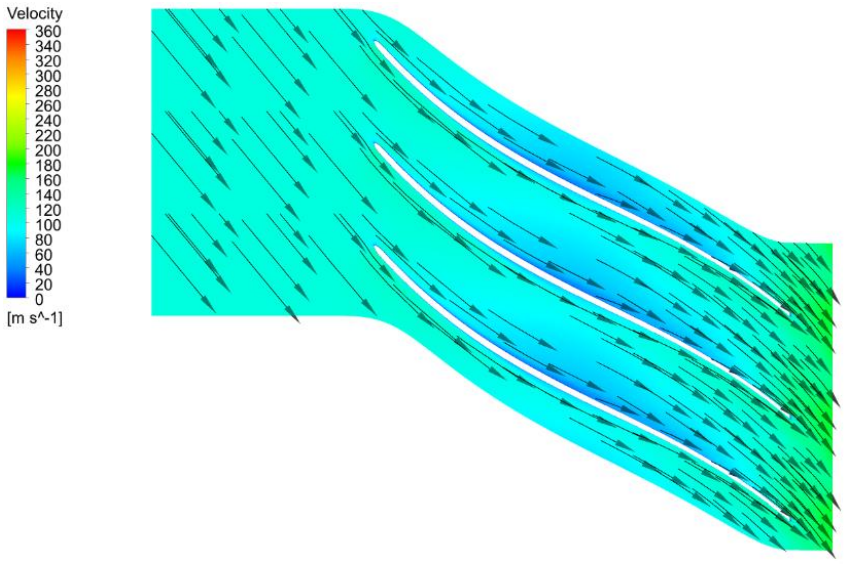

Figure 12. Velocity at span of 50%, blade to blade.

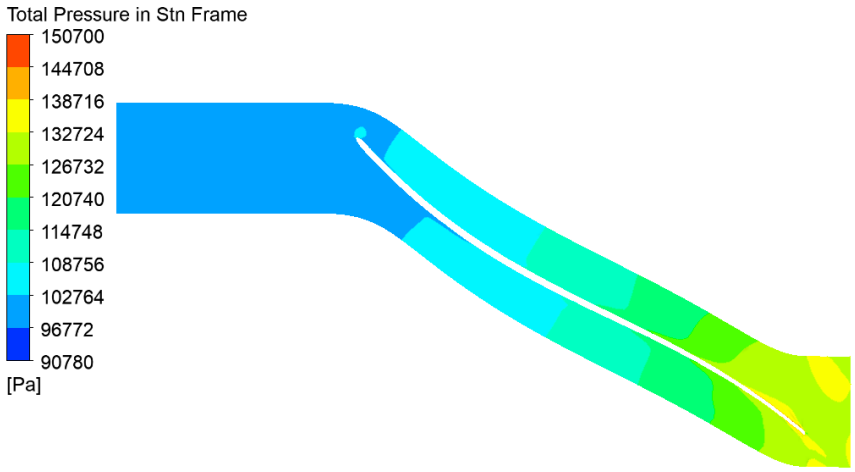

Figure 13. Total pressure contour.

Table 5. Percentage errors of pressure ratios.

Mass Flow Rate from Analysis (kg/s)	Pressure Ratio from Analysis	Experimental Pressure Ratio	Experimental Mass Flow Rate (kg/s)	Errors %
0.341	1.414	1.386	0.341	1.98
0.377	1.4011	1.385	0.377	1.15
0.428	1.3878	1.383	0.428	0.35
0.509	1.3691	1.38	0.509	0.80
0.622	1.3383	1.355	0.622	1.25
0.789	1.2999	1.306	0.789	0.47
0.969	1.2397	1.223	0.969	1.35

As seen in Table 5, there is agreement between the results we obtained from numerical analysis and the experimental results in the literature.

As can be seen in Figure 14, our numerical analysis is compatible with the experimental results. Thus, it is accepted that the numerical analysis results of the tandem blade radial compressor to be designed will be correct.

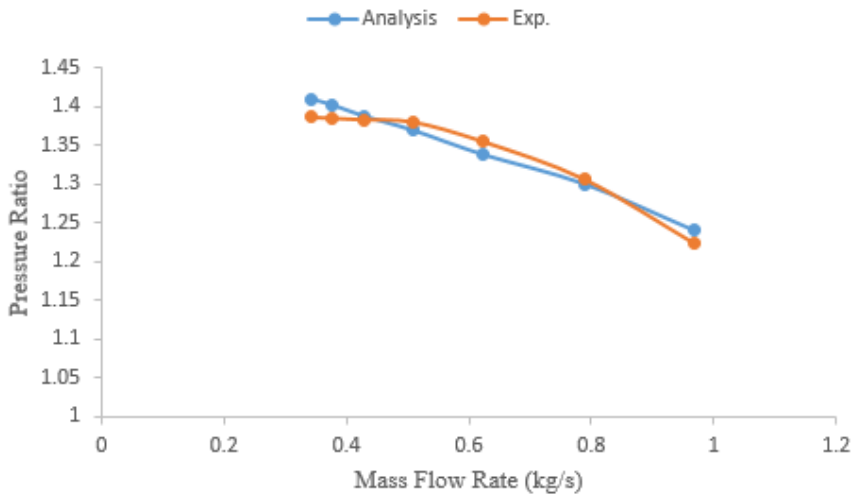

Figure 14. Experimental results and analysis results.

Optimization Results

In the response surface method of the response surface optimization module, the values of the output parameters can be seen according to the values of the input parameters. The values of the parameters for the efficiency of the output parameters are shown in Figure 15.

As seen from Figure 15, the efficiency value is at its highest at the point where the X value is one. It is seen that the efficiency is at its lowest value when the x value is three. It is seen that the C value has the lowest value of efficiency at an angle of 5 degrees. It can be seen from the graph that the highest efficiency values are between 1–2 and 8–9. For the L parameter, it is seen that the efficiency is highest at 15 mm. It is understood from the graph that as the L value increases, the efficiency decreases. For the theta angle, it is seen that the efficiency is at its highest value at an angle of 85 degrees, and the efficiency is at its lowest at an angle of 60 degrees, which is the initial value.

The graphs of the values of these parameters in the same module, corresponding to the total pressure ratio, are also shown in Figure 16.

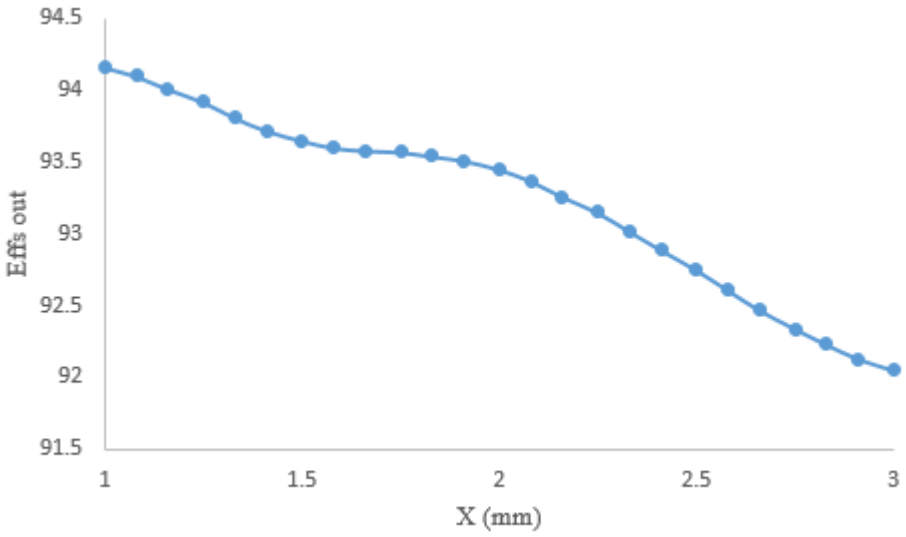

Figure 15. *Cont.*

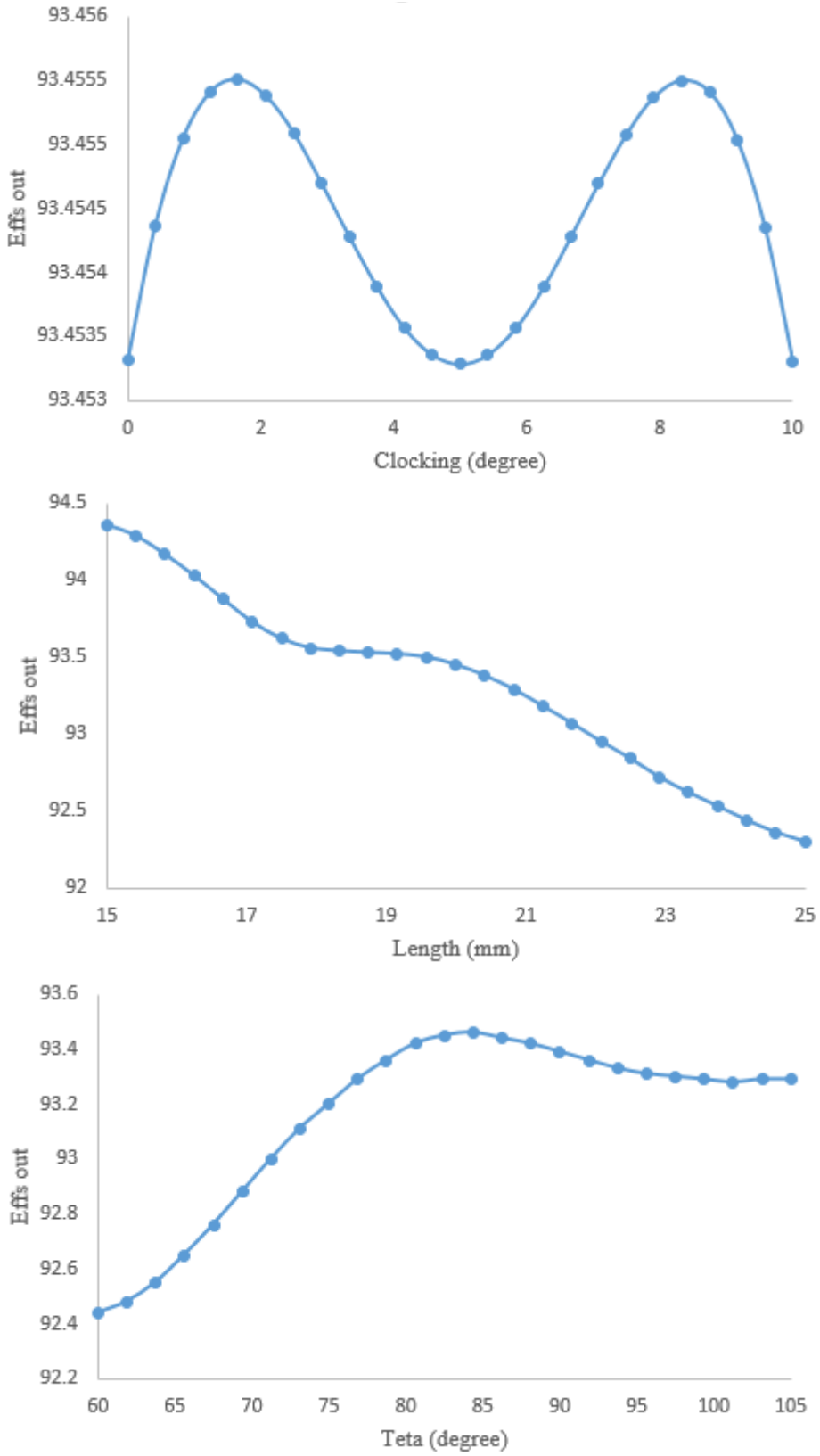

Figure 15. Efficiency result curves of X, C, L, and θ parameters, respectively.

In Figure 16, the X value takes values between the lower and upper limits we determined and the total pressure ratios corresponding to these values can be seen from the graph. Even though it does not increase linearly, it is seen that the total pressure ratio

decreases as the distance between the inducer and exducer increases. If we examine the clocking C value, it is expected that there will be a curve that constantly repeats itself at angles, since it is the horizontal distance between the inducer and the exducer. It is seen that the pressure compression ratio decreases as the inducer height value increases, starting from 15 mm. It is seen that it has its lowest value at the upper value of 25 mm. It is seen that the total pressure ratio first increases and then decreases as the theta degree increases. It can be seen from the graph that it has the highest value at a cutting angle of 85 degrees.

In the optimization module, the last module of the response surface method, optimization processes were started by targeting the values with the highest pressure compression ratio and efficiency. The multi-objective genetic algorithm (MOGA) method was used as the optimization method. The MOGA method is a variant of NSGA-II based on controlled elitism. This method supports multiple objectives and constraints and aims to find the global optimum. In this study, we aim to find the maximum values of the output parameters when there are no restrictions. With this method, 4000 design points were created initially, and continued with 800 design points in each iteration. Three optimum designs were obtained in a maximum of 20 iterations. The values of the optimum design points are shown in Table 6. The design points with the parameter values in Table 6 are the optimum points that give the highest total pressure ratio and efficiency.

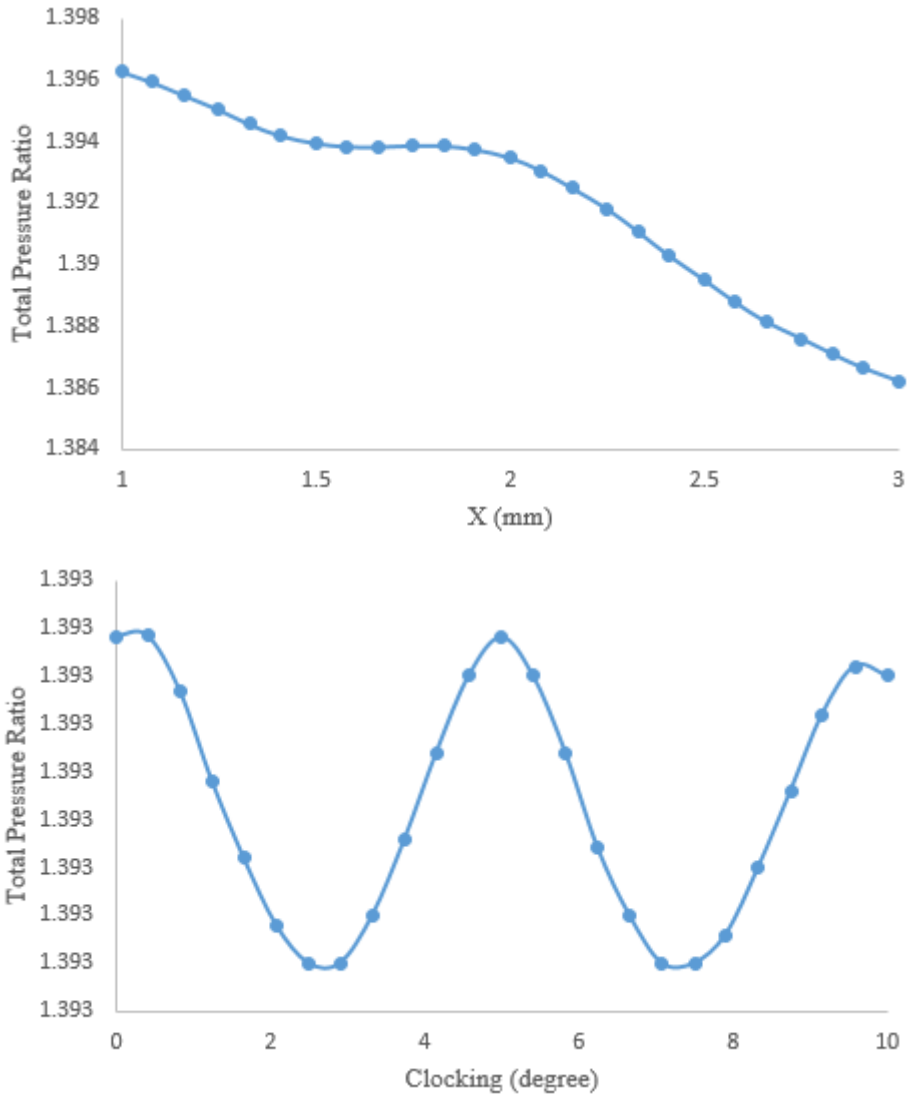

Figure 16. *Cont.*

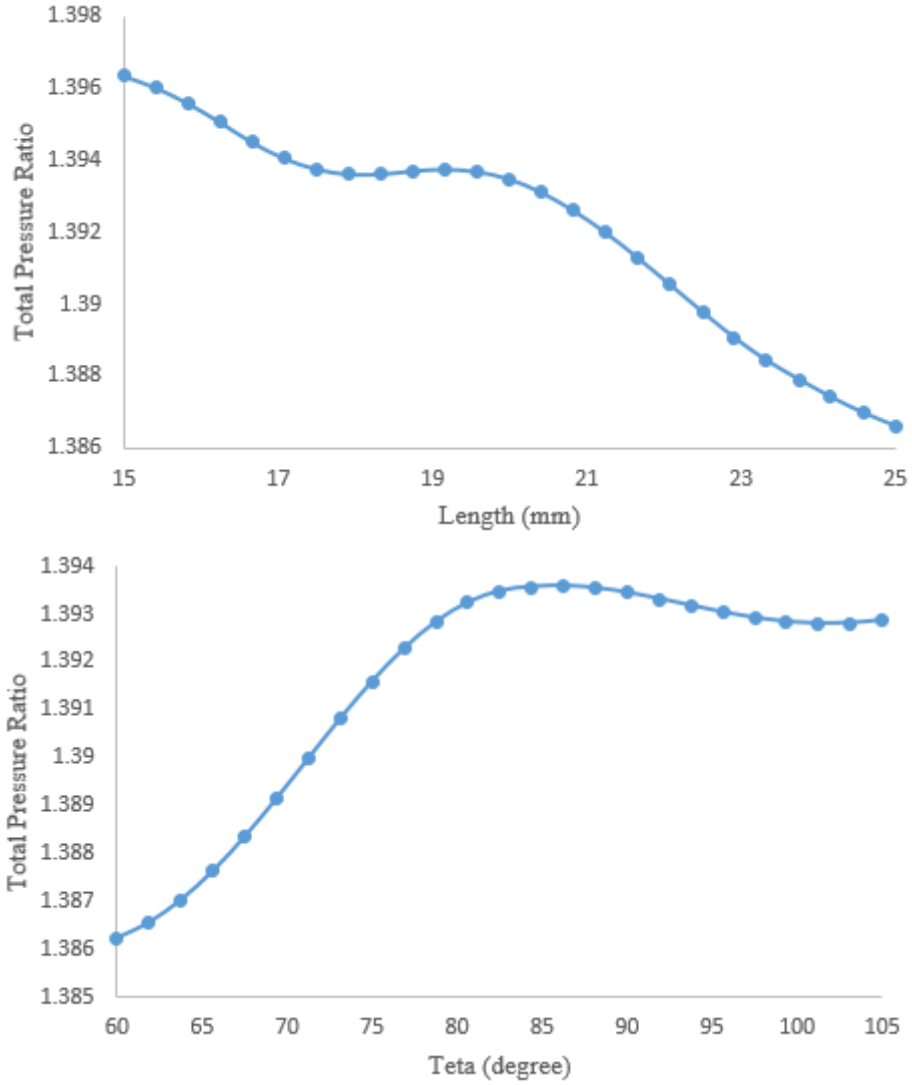

Figure 16. Pressure compression ratio result curves of X, C, L, and θ parameters, respectively.

Table 6. Top three design points.

	Design Point 1	Design Point 2	Design Point 3
θ (°)	76.166	75.398	77.616
X (mm)	1.001	1.0002	1.0003
C (°)	5.0217	5.0217	5.3439
L (mm)	15.005	15.005	15.005
Efficiency	94.61	94.609	94.61
Total Pressure Ratio	1.3985	1.3986	1.3985

Since the values and results were very close, design number 1 was selected from these design points, geometry was created accordingly, and analyses were made at different flow rates. The geometry of design number 1 is shown in Figure 17.

Analyses at different flow rates were carried out using the analysis method, whose accuracy we have previously confirmed through the experimental results. The flow rates used in the analyses and the values obtained from the analysis results are shown in Table 7.

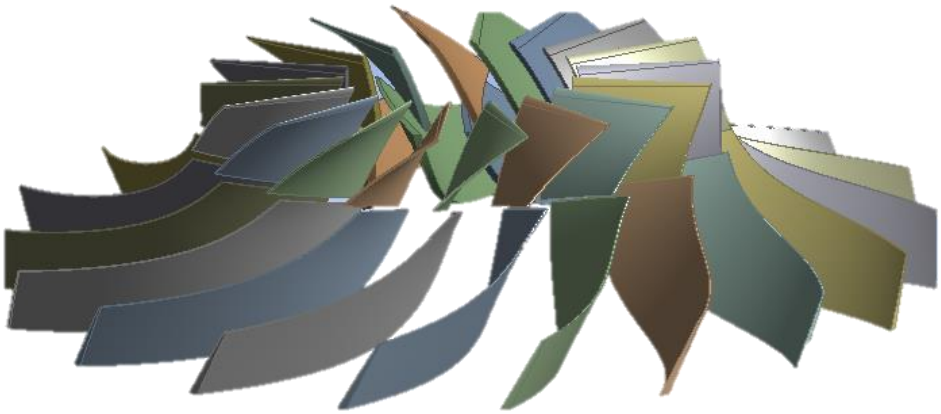

Figure 17. Optimum design geometry.

Table 7. Flow rate and analysis results.

Mass Flow Rate (kg/s)	Tandem Opt. Pr.	Tandem Pr.	Conventional Blade Pr.
0.341	1.4499	1.4493	1.41
0.377	1.4465	1.4448	1.4018
0.509	1.441	1.4371	1.3691
0.622	1.427	1.4153	1.3383
0.789	1.3945	1.3896	1.2999
0.969	1.3525	1.35	1.2397

The graphical results of the optimum tandem blade design, tandem blade design, and conventional blade design at the same speed and different flow rates are shown in Figure 18.

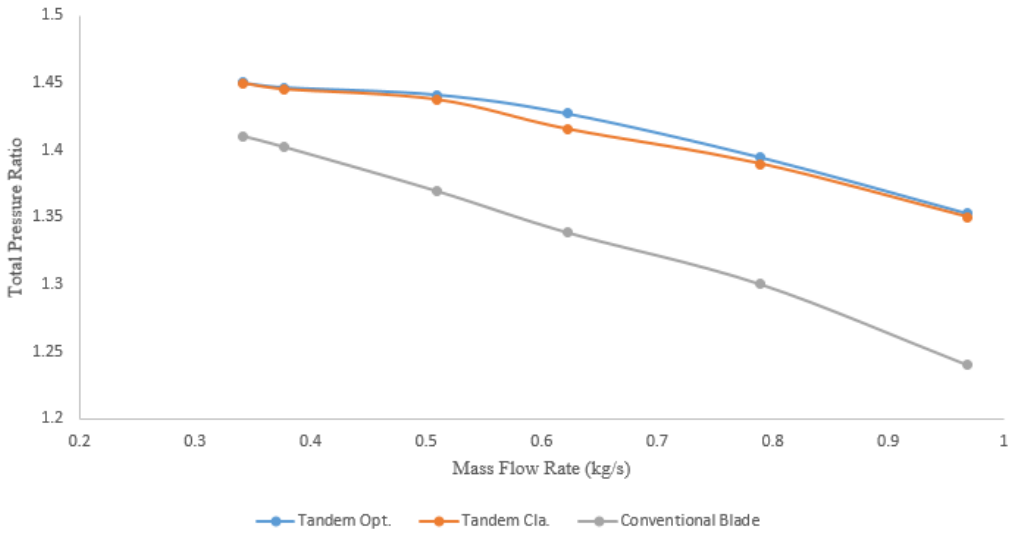

Figure 18. Comparison of analysis results.

The analysis results of the optimum tandem-bladed impeller give better results than the classical tandem blade and conventional blade impellers.

4. Conclusions

A radial compressor with test results available in the literature was designed, and numerical analysis was performed using the package program. It has been observed that the current test results and the numerical analysis results are pretty close. There is a maximum error rate of 1.98% and a minimum of 0.35% between the numerical analysis and experimental results.

After seeing that the test results of the conventional blade radial compressor in the literature were compatible with the results of our numerical analysis, we performed the analysis of our tandem blade radial compressor with four input parameters. Design points were created within the determined lower and upper limits. Three different optimum designs with the highest output parameters, total pressure ratio, and efficiency were obtained using the MOGA optimization method. With this method, 4000 design points were initially created to find the optimum design, and optimum designs were obtained in a total of 20 iterations, each containing 800 design points. Numerical analyses were carried out according to design point one of these obtained design points. The parameter values of the design point one with the highest performance were found to be theta angle 76.166°, X value 1.001 mm, clocking C angle 5.0217°, and L value 15.005 mm. The efficiency of this design point 1 was found to be 94.61 and the total pressure ratio was 1.3985. As a result of these analyses at different flow rates, it has been seen that the performance of our optimum TB centrifugal compressor is better than the TB and conventional blade radial compressor.

Author Contributions: Methodology, M.E.S., R.B. and Z.P.; Validation, M.E.S.; Writing—original draft, M.E.S.; Writing—review & editing, R.B. and Z.P.; Supervision, M.E.S. All authors have read and agreed to the published version of the manuscript.

Funding: This research received no external funding.

Data Availability Statement: The original contributions presented in the study are included in the article, further inquiries can be directed to the corresponding author.

Conflicts of Interest: The authors declare no conflict of interest.

References

1. Yoon, S.Y.; Lin, Z.; Lim, K.T.; Goyne, C.; Allaire, P.E. Model validation for an AMB-based compressor surge control test rig. In Proceedings of the 48h IEEE Conference on Decision and Control (CDC) Held Jointly with 2009 28th Chinese Control Conference, Shanghai, China, 15–18 December 2009; pp. 756–761.
2. Boyce, M.P. Principles of Operation and Performance Estimation of Centrifugal Compressors. In Proceedings of the 22nd Turbomachinery Symposium, Houston, TX, USA, 14–16 September 1993; pp. 161–177.
3. Kulkarni, V.V.; Anil, T.R.; Rajan, N.K.S. An Impeller Blade Analysis of Centrifugal Gas Compressor Using CFD. *Int. J. Innov. Eng. Technol.* **2016**, *7*, 217–223.
4. Xu, C.; Yang, H.; Jiang, Y.; Yi, Z. The development of an integrally geared centrifugal compressor. *Int. J. Fluid Mech. Therm. Sci.* **2019**, *5*, 1–9. [CrossRef]
5. Xu, C.; Amano, R.S. Study of the flow in centrifugal compressor. *Int. J. Fluid Mach. Syst.* **2010**, *3*, 260–270. [CrossRef]
6. Xu, C.; Amano, R.S. The development of a centrifugal compressor impeller. *Int. J. Comput. Methods Eng. Sci. Mech.* **2009**, *10*, 290–301. [CrossRef]
7. Xu, C.; Amano, R.S. Empirical design considerations for industrial centrifugal compressors. *Int. J. Rotating Mach.* **2012**, *2012*, 184061. [CrossRef]
8. Mostefa, B.; Kaddour, R.; Embarek, D.; Amar, K. Analysis and Optimization of the Performances of the Centrifugal Compressor Using the CFD. *Int. J. Heat Technol.* **2021**, *39*, 107–120. [CrossRef]
9. Aungier, R.H. *Centrifugal Compressors: A Strategy for Aerodynamics Design and Analysis*; ASME: New York, NY, USA, 2000. [CrossRef]
10. Xu, C. Design Experience and Considerations for Centrifugal Compressor Development. *Proc. Inst. Mech. Eng. Part G J. Aerosp. Eng.* **2007**, *221*, 273–287. [CrossRef]
11. Hadavandi, R.; Fontaneto, F.; Desset, J. Complete characterization of a highly loaded low pressure compressor at different reynolds numbers for computational fluid dynamics simulations. *J. Turbomach.* **2018**, *140*, 061008. [CrossRef]
12. Shaaban, S. Design optimization of a centrifugal compressor vaneless diffuser. *Int. J. Refrig.* **2015**, *60*, 142–154. [CrossRef]
13. Sun, J.; Ding, J.; Chen, S.; Li, J. Numerical Simulation of centrifugal compressor impeller flow flied based on ANSYS Workbench. In Proceedings of the 5th International Conference on Advanced Design and Manufacturing Engineering Atlantis Press, Shenzhen, China, 19–20 September 2015; pp. 449–453.
14. Xu, C.; Amano, R.S. Centrifugal compressor performance improvements through impeller splitter location. *J. Energy Resour. Technol.* **2018**, *140*, 051201. [CrossRef]
15. Li, J.; Yin, Y.; Li, S.; Zhang, J. Numerical simulation investigation on centrifugal compressor performance of turbocharger. *J. Mech. Sci. Technol.* **2013**, *27*, 1597–1601. [CrossRef]
16. Aghaei tog, R.; Mesgharpoor Tousi, A.; Soltani, M. Design and CFD analysis of centrifugal compressor for a microgasturbine. *Aircr. Eng. Aerosp. Technol.* **2007**, *79*, 137–143. [CrossRef]

17. Roberts, D.A.; Kacker, S.C. Numerical investigation of tandem-impeller designs for a gas turbine compressor. *J. Turbomach.* **2002**, *124*, 36–44. [CrossRef]
18. Cuturi, N.; Sciubba, E. Design of a Tandem Compressor for the Electrically-Driven Turbocharger of a Hybrid City Car. *Energies* **2021**, *14*, 2890. [CrossRef]
19. Noman Danish, S.; Ud-Din Khan, S.; Umer, U.; Rehman Qureshi, S.; Ma, C. Performance evaluation of tandem bladed centrifugal compressor. *Eng. Appl. Comput. Fluid Mech.* **2014**, *8*, 382–395. [CrossRef]
20. Ju, Y.; Zhang, C. Multi-objective optimization design method for tandem compressor cascade at design and off design conditions. In Proceedings of the Turbo Expo: Power for Land, Sea, and Air, Glasgow, UK, 22 December 2010; Volume 44021, pp. 785–796.
21. Josuhn-Kadner, B. Flow Field and Performance of a Centrifugal Compressor Rotor with Tandem Blades of Adjustable Geometry. In Proceedings of the Turbo Expo: Power for Land, Sea, and Air, American Society of Mechanical Engineers, Hague, The Netherlands, 13–16 June 1994; Volume 78835, p. V001T01A004.
22. Josuhn-Kadner, B.; Hoffmann, B. Investigations on a radial compressor tandem-rotor stage with adjustable geometry. In Proceedings of the 37th ASME International Gas Turbine and Aeroengine Congress and Exposition, Cologne, Germany, 1–4 June 1993; ASME Paper 92-GT-218, pp. 552–559.
23. Li, Z.; Wu, Y.; Lu, X. Performance Improvement of a Highly Loaded Transonic Centrifugal Compressor with Tandem Impeller and Freeform Blade Configuration. *Energies* **2022**, *15*, 9283. [CrossRef]
24. Li, Z.; Han, G.; Lu, X.; Huang, E.; Zhao, S. Improving the operating range using a centrifugal compressor with a tandem impeller. *Aerosp. Sci. Technol.* **2020**, *96*, 105548. [CrossRef]
25. Sadagopan, A.; Camci, C. A design strategy for a 6: 1 supersonic mixed-flow compressor stage. *Aerosp. Sci. Technol.* **2019**, *87*, 265–277. [CrossRef]
26. Sadagopan, A.; Camci, C. Viscous flow and performance issues in a 6: 1 supersonic mixed-flow compressor with a tandem diffuser. *Aerosp. Sci. Technol.* **2019**, *88*, 9–21. [CrossRef]
27. Cravero, C.; Marsano, D.; Sishtla, V.; Halbe, C.; Cousins, W.T. Numerical Investigations of Near Surge Operating Conditions in a Two-Stage Radial Compressor with Refrigerant Gas. *J. Eng. Gas Turbines Power* **2024**, *146*, 1–47. [CrossRef]
28. Zhu, W.; Ren, X.D.; Li, X.S.; Gu, C.W. Analysis and improvement of a two-stage centrifugal compressor used in an MW-level gas turbine. *Appl. Sci.* **2018**, *8*, 1347. [CrossRef]
29. Ahmad, N.; Bin, J.; Qun, Z.; Abdu Ahmad, S.; Fawzy, H. Performance enhancement of a transonic axial flow compressor with circumferential casing grooves to improve the stall margin. *J. Appl. Fluid Mech.* **2020**, *13*, 221–232. [CrossRef]
30. Ahmad, N.; Zheng, Q.; Fawzy, H.; Jiang, B.; Ahmed, S.A. Performance improvement of axial compressor by introduction of circumferential grooves. *Energy Sources Part A Recovery Util. Environ. Eff.* **2020**, 1–21. [CrossRef]
31. Ahmad, N.; Zheng, Q.; Fawzy, H.; Lin, A.; Jiang, B. CFD investigation of an axial compressor with casing treatment for the enhancement of the stall margin. *Sci. Iran.* **2021**, *28*, 3156–3167. [CrossRef]
32. ANSYS Documentation, ANSYS CFX Theory Guide. ANSYS Help. 2017. Available online: https://www.ansys.com/ (accessed on 1 May 2024).
33. Mojaddam, M.; Moussavi Torshizi, S.A. Design and optimization of meridional profiles for the impeller of centrifugal compressors. *J. Mech. Sci. Technol.* **2017**, *31*, 4853–4861. [CrossRef]